

# High-Resolution and Jamming-Resistant Adaptive Synthetic Aperture Radar Imaging System based on UWB-OFDM Waveform

Md Anowar Hossain, Ibrahim Elshafiey, and Majeed A. S. Alkanhal

Department of Electrical Engineering  
King Saud University, Riyadh, Kingdom of Saudi Arabia  
ahossain@ksu.edu.sa, ishafiey@ksu.edu.sa, majeed@ksu.edu.sa

**Abstract**— A novel approach for jamming-resistant and high-resolution synthetic aperture radar (SAR) imaging technique is explored based on ultra-wideband orthogonal frequency division multiplexing (UWB-OFDM) waveform. Suitable waveforms for both friendly and hostile environment are proposed based on various random sequences and tested for SAR imaging in presence of a digital radio frequency memory (DRFM) repeat jammer. Adaptivity factor is introduced to make the system consistent in both environments. Wide-band ambiguity function (WAF) has been derived and the effect of sub-carrier composition in UWB-OFDM waveform as SAR signal is analyzed to avoid ambiguity in image reconstruction. Appropriate UWB-OFDM pulse shaping is introduced for SAR imaging in jamming scenarios and in hostile environments to solve the susceptibility of conventional linear frequency modulated (LFM) chirp signal, Gaussian pulses and any other constant pulse shape to avoid the possibility of false target introduced by jammer and to achieve secured imaging in jamming scenarios. The peak side-lobe performance is examined in terms of number of OFDM sub-carriers and sub-carrier orientation.

**Index Terms** — Orthogonal frequency division multiplexing (OFDM), synthetic aperture radar (SAR), SAR jamming and anti-jamming, and ultra-wideband (UWB).

## I. INTRODUCTION

Synthetic aperture radar (SAR) is used to obtain high resolution images of a large target area. It involves transmitting signals at spaced intervals called pulse repetition interval (PRI). The

responses at each PRI are stored and processed to reconstruct a radar image of the terrain [1]. Recently, achievement of high resolution SAR images has been investigated depending on transmission of ultra-wideband (UWB) waveform as radar signals [2]. UWB technology has double advantages: good penetration capability and high resolution target detection for radar applications [3] and [4].

Conventional LFM chirp signal experiences high susceptibility to jammer because of the linear nature of the intermediate frequency (IF). Gaussian pulse exhibits constant pulse-shape make these pulses susceptible to certain forms of deception jamming. These radars may be susceptible to certain types of jammer in scenarios where multiple pulse transmissions are mandatory, as in SAR imaging. Constant pulse shape also prevents using multiple radars in same location as they could interfere with each other. Therefore, it is necessary to explore radar signals that employ wide bandwidths and have the ability to quickly adjust to any adverse situations.

Orthogonal frequency division multiplexing (OFDM) is a method of digital modulation commonly used in commercial communications, shows great potential to be used in radar pulse shaping. Although OFDM has been frequently studied and commercialized in the digital communication field, it has not so widely been studied by radar communities rather than a few efforts [5-10]. An OFDM signal consists of several orthogonal sub-carriers that are simultaneously passed over a single transmission path. Each sub-carrier contains a small portion of the entire signal bandwidth [11]. Spectral components in OFDM signals are orthogonal to each other; therefore, by

controlling the sub-carriers we can ensure that any two waveforms emitted simultaneously will have minimum interference. Essentially, the subcarriers partition the bandwidth of the signal into several smaller orthogonal blocks. The system has control over the sub-carriers and, therefore, control over the spectrum of the waveform. In radar scenarios, the spectrum can be manipulated to avoid any interference that may be introduced from hostile environments. Moreover, OFDM signals can be formed in an attempt to eliminate all forms of jamming and interference.

In some scenarios, enemy combatants may use specific electronic countermeasures (ECM) to confuse the radar by altering the radar received signal characteristics resulting in a poor reconstructed image [12]. Pulse diversity of radar signals is an effective electronic counter-countermeasures (ECCM) technique against deception jammers. Advances in sampling technology have increased sampling speed allowing for OFDM waveforms employing UWB (500 MHz and above) to be generated accurately and at relatively low costs. The wide bandwidth along with excellent pulse diversity shows clear potential for UWB-OFDM signal to be used as radar pulse in jamming scenarios. The advantages of using OFDM waveform in radar application are: a) waveforms are generated digitally with pulse-to-pulse shape variation, b) ease of jamming/interference mitigation, and c) noise-like waveforms provide low probability of interception (LPI) and low probability of detection (LPD).

The structure of the paper is as follows. UWB-OFDM signal generation is described in section II, while the proposed multi-modulation technique is presented in section III. Detailed analysis of DRFM repeat jammer is discussed in section IV. Target model based on different scenarios is presented in section V. Section VI presents the comparison of auto-correlation and cross-correlation of different pulses in radar perspective. SAR imaging in jamming scenarios is investigated in section VII and wideband ambiguity function is derived in section VIII. Conclusions are provided in section IX.

## II. UWB-OFDM SIGNAL GENERATION

UWB-OFDM signal is generated according to the scheme shown in Fig. 1 by randomly populating the digital frequency domain vector as,

$$\Psi_{\omega} = [\Pi_{ns} \Pi_0 \Pi_{ps}] \quad (1)$$

where,  $\Pi_{ps}$  and  $\Pi_{ns}$  represent the positive and negative sub-carriers, respectively, whereas  $\Pi_0$  represents the baseband DC value. Inverse discrete Fourier transform (IDFT) is then applied to  $\Psi_{\omega}$  to get the discrete time domain OFDM signal as,

$$\Psi_{tx}(t) = F^{-1}[\Psi_{\omega}] \quad (2)$$

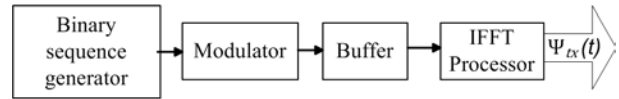
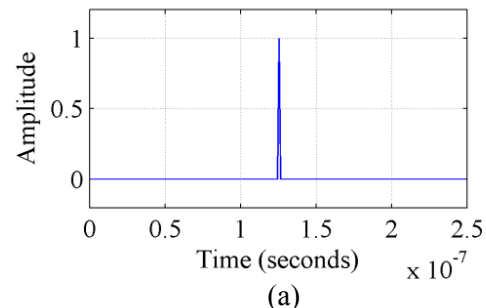


Fig. 1. UWB-OFDM signal generator.

UWB-OFDM waveforms are generated using the following parameters: number of OFDM sub-carriers = 256, sampling time,  $\Delta t_s = 1\text{ns}$  results in baseband bandwidth,  $B_0 = 1/2\Delta t_s = 500\text{MHz}$ , dividing by a factor of two to satisfy Nyquist criterion. Observing Fig. 2 (a) we see that when  $\Pi_{ps}$  is populated with all 1's and modulation scheme is chosen as BPSK, UWB-OFDM waveform becomes a short spike i.e., delta pulse, which can provide the best possible range resolution and exact position of the target in radar application. Hardware limitations can be an obstacle to generate this waveform, however, similar performance can be achieved by employing the samples of an LFM chirp in OFDM context as shown in Fig. 2 (b). We can consider these signals for the SAR imaging in friendly environment to obtain high resolution images. However, the constant pulse shape causes the system to suffer in jamming scenarios. Figure 3 shows an UWB-OFDM waveform when  $\Pi_{ps}$  populated randomly with 1's and 0's and modulation scheme is chosen as BPSK. It is observed that the signal is noise-like and provides a unique signal at each PRI, ideal for the SAR system in jamming scenarios.



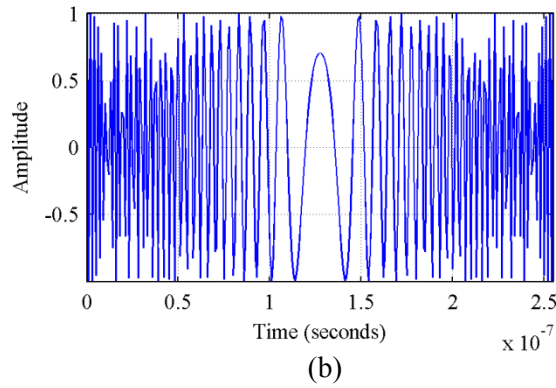


Fig. 2. UWB radar signal a) OFDM waveform with all sub-carriers and b) OFDM-LFM chirp.

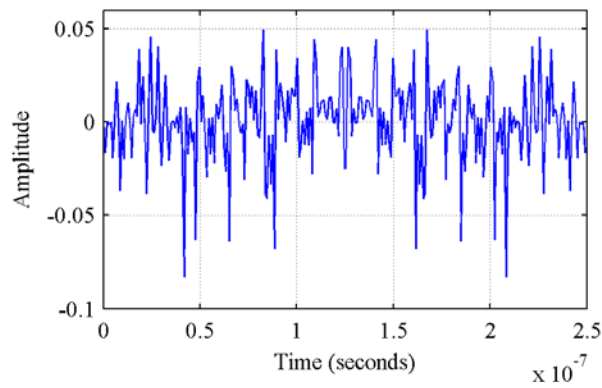


Fig. 3. UWB-OFDM signal with random sub-carrier orientation.

### III. RANDOM MODULATION

Random modulation or multi-modulation modem modulates and demodulates signals using multiple modulation schemes. It includes a modulation selector unit that selects respective ones of the set of modulations to modulate the signals. Figure 4 shows the block diagram of the multi-modulated UWB-OFDM signal generator. The modulation selector fixed an arbitrary  $M$ -ary PSK from  $M = 2^n$  and the random data generator generates a sample between 0 to  $(M-1)$ . The sample is then modulated according to the selected modulation scheme and stored in a buffer. IFFT is then applied to the frequency domain vector to obtain the discrete time-domain UWB-OFDM signal.

Figure 5 shows an UWB-OFDM waveform using multi-modulation technique in which different modulation schemes are employed for the individual OFDM sub-carriers. It is observed that the signal is noise-like and provides high degree of randomness, suitable for the SAR system in hostile environments. Even jammer cannot identify the modulation scheme used in generating the waveform because the signal is inherently multi-modulated.

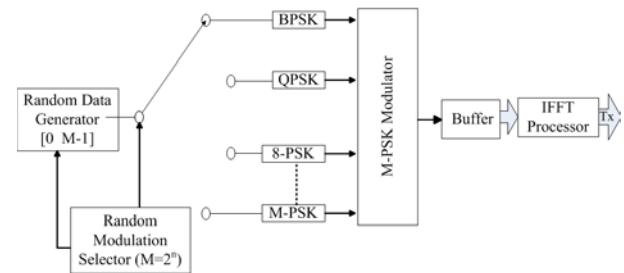


Fig. 4. UWB-OFDM signal generator with multi-modulation.

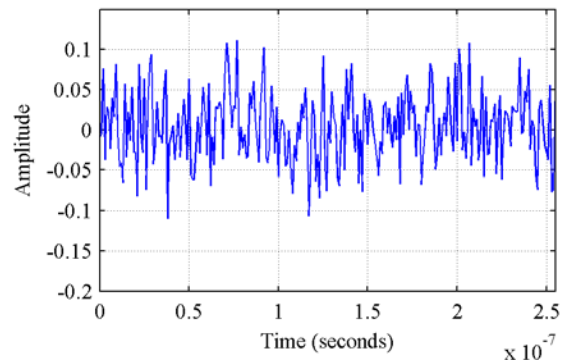


Fig. 5. Multi-modulated UWB-OFDM signal.

### IV. DRFM JAMMER CONCEPTS

Deception jammers attempt to manipulate transmitted SAR signals in order to introduce false target into the reconstructed SAR image. This type of jamming can be accomplished by using a digital radio frequency memory (DRFM) repeat jammer [12] as shown in Fig. 6. The radar transmitted signal is received and converted to baseband. Analog-to-digital conversion is then performed to produce the discrete signal. A delay is then introduced to the discrete signal creating a false range offset by means of a controller and stored in memory until the next predicted PRI.

The discrete delayed signal is then passed through a digital-to-analog (DAC) converter and is mixed with an exponential at the known center frequency results in the transmitted jammer signal (received signal for radar) given by,

$$J_{tx}(t, u) = \sum_{n=1}^{N_j} \Psi_{txj}(t - t_{dj}) \quad (3)$$

where,  $t_{dj} = \frac{2}{c} \sqrt{(X_j - x_j)^2 + (y_j - u)^2}$  denotes the jammer introduced time delay and  $(x_j, y_j)$  is the position of the false target.  $X_j$  and  $u$  represents the jammer distance to swath and the synthetic aperture positions respectively while  $j = 1, 2, 3, \dots, N_j$  are the number of false target reflections at any given synthetic aperture position and  $c$  is the speed of light. The term  $\Psi_{txj}$  is the cyclic shifted version of the radar transmitted signal.

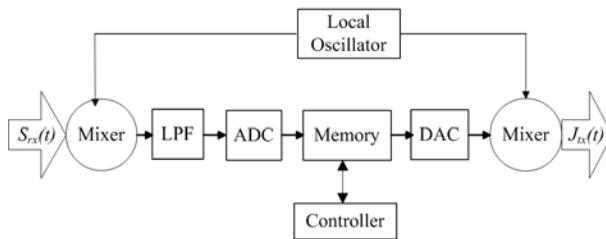


Fig. 6. DRFM repeat jammer.

If center frequency is known to the jammer and it is capable to form exact replicas of the transmitted SAR signal, the received signal for radar in jamming scenarios is given by

$$\Psi_{rxj}(t, u) = \sum_{n=1}^{N_a} \sigma_n \Psi_{tx}(t - t_{dn}) + J_{tx}(t, u) + \eta(t), \quad (4)$$

where,  $t_{dn} = \frac{2}{c} \sqrt{(X_c - x_n)^2 + (y_n - u)^2}$  denotes the time-delay associated with the actual target position  $(x_n, y_n)$  and  $X_c$  is the range distance to center of the swath. Where,  $n = 1, 2, 3, \dots, N_a$  are the number of actual target reflections at any given synthetic aperture position while  $\sigma_n$  denotes the reflectivity of the target. The term  $\Psi_{tx}$  is the radar transmitted signal and  $\eta(t)$  denotes the additive white Gaussian noise, respectively.

## V. TARGET MODEL

In practice, reflection from a point target is not a single peak as shown in Fig. 7 (a); the radar received signal is the combination of reflection from the target and closely surrounded scatterers of radar cross section (RCS) of a target as shown in Fig. 7 (b). Other important parameters that can be considered in target model are surface clutter and free space path loss. Table 1 shows the parameters used for simulation of the point target.

Surface clutter refers to reflections of a radar signal from land, sea or any other surfaces [13]. To detect targets above the surface, the radar must be able to distinguish between clutter and the targets of interest. For example, the radar should detect targets on the ground while accounting for radar reflections from trees or houses. Fig. 7 (c) shows the target profile based on surface clutter.

Propagation environments have significant effects on the amplitude, phase, and shape of propagating space-time wave-fields. If we consider a system that propagates signals through free space, we can model the free space path loss as,

$$L = \frac{(4\pi R)^2}{\lambda^2} \quad (5)$$

where,  $R$  represents the one-way distance between the target and the radar in meters, and  $\lambda$  is the signal wavelength. The target profile using free space path loss is shown in Fig. 7 (d). We observe that the maximum peak of the point target decreases as the distance increases. Figure 8 shows the clutter returns based on constant gamma model for different types of surface such as flat land, rugged mountain and sea-state.

Table 1: UWB-OFDM SAR simulation parameters.

Parameter	Symbol	Value
Pulse repetition frequency	PRF	300 Hz
Flight Duration	Dur	3 sec
Velocity of platform	$V_p$	200 m/s
Carrier frequency	$f_c$	7.5 GHz
Distance to target area	$X_c$	1Km
Half target area width	$X_0$	600 m

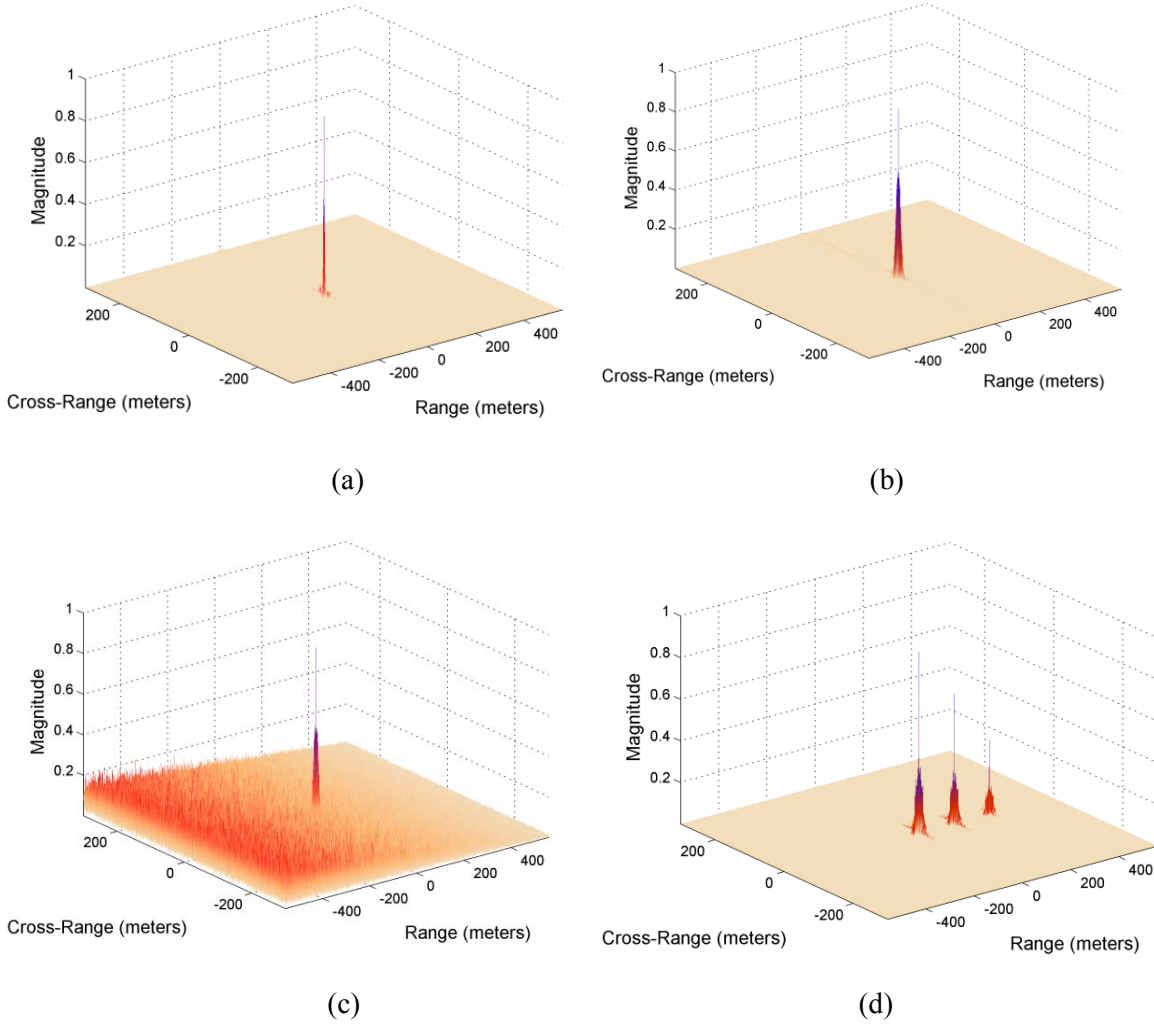


Fig. 7. Target profile for (a) ideal model, (b) RCS model, (c) clutter model, and (d) path loss model.

## VI. WAVEFORM ANALYSIS

Analysis of waveforms is presented in terms of their auto-correlation function (ACF) and cross-correlation function (CCF). The auto-correlation and cross-correlation properties of the sequences used in generating the transmitted waveform play an important role in high resolution SAR imaging and in false target rejection. Cross-correlation is the measure of similarity between two different sequences and can be expressed as,

$$R_{xy}(m) = \begin{cases} \sum_{n=0}^{N-m-1} x_{n+m} y_n^* & m \geq 0 \\ R_{yx}^*(-m) & m < 0 \end{cases} \quad (6)$$

where,  $x_n$  and  $y_n$  are the elements of two different sequences with period  $N$ . Auto-correlation shows the measure of similarity between the sequence

and its cyclic shifted copy, which can be obtained from equation (6) as a special case ( $x = y$ ) [14].

The sequences with better auto-correlation properties provide high resolution target detection and lower cross-correlation properties provide degradation of false target. So, our objective is to find the waveform that provides the lowest cross-correlation properties among all types of sequences. The auto-correlation is measured as the correlation between the received signal and the transmitted signal while cross-correlation is measured as the correlation between received signal and transmitted signal at previous PRI. The auto-correlation and cross-correlation properties are examined for all types of UWB-OFDM pulses in the following subsections assuming a point target at the center of the target area.

### A. Constant pulses

The delta pulse and LFM chirp shown in Figs. 2 (a) and 2 (b) before providing the highest auto-correlation as shown in Figs. 9 (a) and 9 (b), respectively with a main lobe width of 0.32 meters, which almost matches the theoretical range resolution,  $\Delta R = c/2B_0 = 0.30$  meters. These pulses are best suited for the SAR system in friendly environment to obtain high resolution images. However, both pulses also exhibits highest cross-correlation makes them imperfect for the SAR system in jamming scenarios.

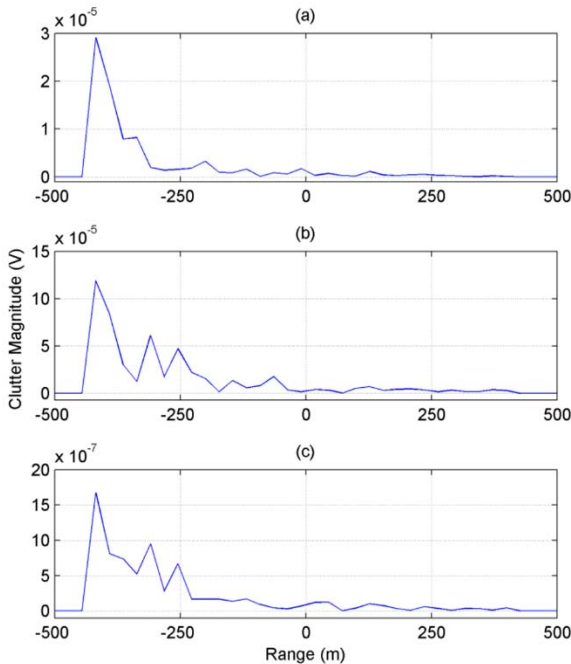


Fig. 8. Clutter return versus the range for (a) flat land, (b) rugged mountain, and (c) sea-state.

### B. Random sequences

Random sequences such as Pseudo-noise (PN) sequences, Gold sequences and Kasami sequences are used extensively in spread-spectrum communication system [14]. We can consider these sequences for noise-like UWB-OFDM waveform generation to be used as SAR transmitted pulse in jamming scenarios. The parameter used in generating the sequences is shown in Table 2. The generator polynomial has been chosen so that the balance between number of 1's and 0's is maintained.

The PN sequences are almost ideal when viewed in terms of their autocorrelation function

as shown in Fig. 10 (a). Unfortunately, the cross-correlation between any pair of PN sequences of the same period can have relatively high peaks that are undesirable as shown in Fig. 10 (b). A particular class of PN sequences called Gold sequences provides better cross-correlation properties and is generated by modulo-2 addition of two PN sequences of the same length. The auto-correlation and cross-correlation of Gold sequences is shown in Figs. 10 (c) and 10 (d), respectively.

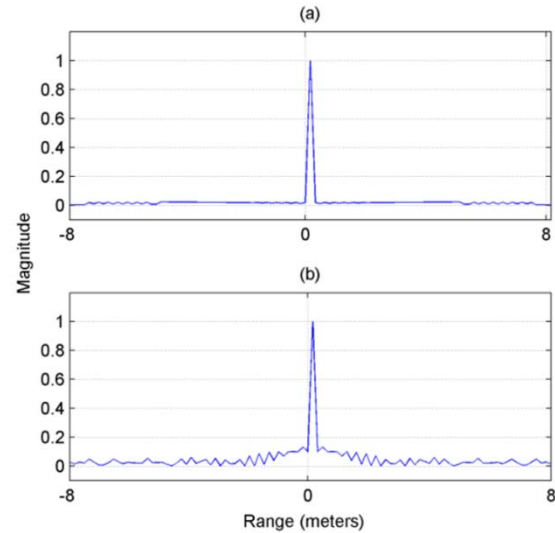


Fig. 9. Point target profile for a) UWB-OFDM pulse with all sub-carriers (ACF) and b) UWB OFDM-LFM chirp (ACF).

Table 2: Sequence generator parameters.

Sequence Generator	Generator polynomial	Initial states
PN	[53 6 2 0]	[53 41 28 15 1]
Gold	[11 2 0]	[11 8 4]
	[11 8 5 2 0]	[11 7 3]
Kasami	[12 6 4 0]	[12 8 2 0]

Kasami sequences are one of the important types of binary sequences because of their very low cross-correlation. Kasami sequences provide better cross-correlation as compared to PN sequences and Gold sequences. Figures 10 (e) and 10 (f) show the ACF and CCF of Kasami sequences, respectively.

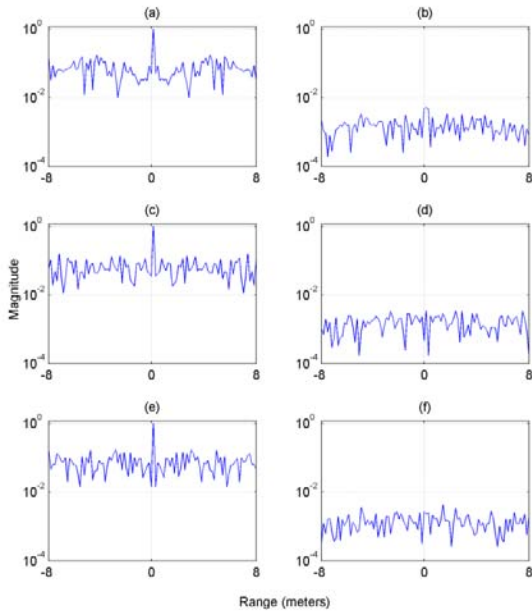


Fig. 10. Point target profile using (a) PN seq. (ACF), (b) PN seq. (CCF), (c) Gold seq. (ACF), (d) Gold seq. (CCF), (e) Kasami seq. (ACF), and (f) Kasami seq. (CCF).

### C. Orthogonal sequences

Orthogonality is the most important properties of Walsh-Hadamard sequences. Because of this property, the cross-correlation between any two codes of the same set is zero, when the system is perfectly synchronized as shown in Fig. 11. Unfortunately, these sequences have non-zero off-peak auto-correlations and cross-correlation in asynchronous case. Figures 12 (a) and 12 (c) show the auto-correlation and cross-correlation in terms of a point target using Walsh-Hadamard sequences without spreading. By spreading Walsh sequences with a PN sequence using specific spreading factor better performance can be achieved.

The spreading uses a waveform that appears random to anyone except the intended receiver of the transmitted signal. The waveform is actually pseudo-random in the sense that it can be generated by precise rules yet has the statistical properties of a truly random sequence. Figures 12 (b) and 12 (d) show the auto-correlation and cross-correlation in terms of a point target using Walsh-Hadamard sequences with spreading by a factor of 4.

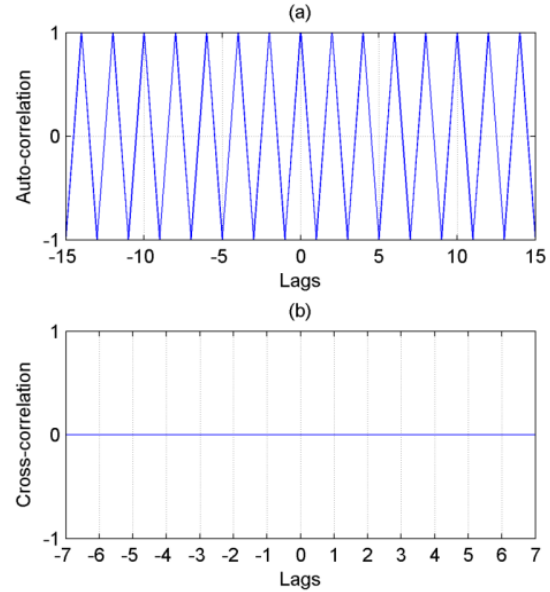


Fig. 11. Ideal Walsh-Hadamard sequences, (a) ACF and (b) CCF.

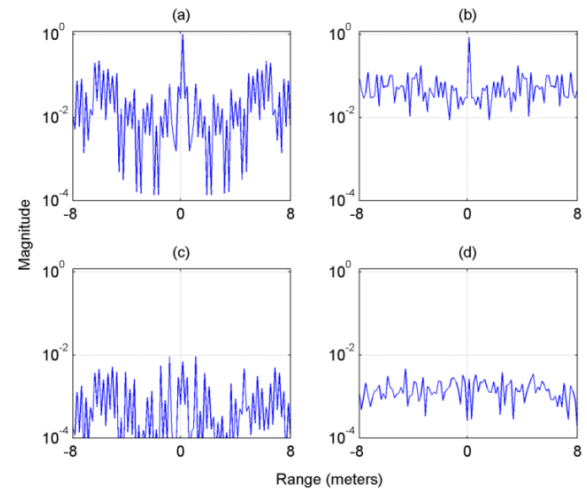


Fig. 12. Point target profile using Walsh-Hadamard sequences showing (a) ACF without spreading, (b) ACF with spreading, (c) CCF without spreading, and (d) CCF with spreading.

### D. Multi-modulated pulse

The proposed multi-modulated UWB-OFDM pulse provides reasonable auto-correlation properties with increased main-lobe width but exhibits lowest cross-correlation as shown in Fig. 13 among all types of pulses makes this pulse ideal for the SAR system for false target rejection.

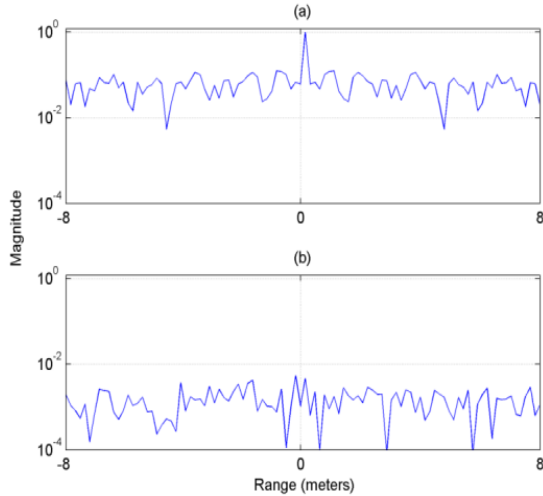


Fig. 13. Point target profile of Multi-modulation (a) ACF and (b) CCF.

Since all cross-correlation values, not just peak values, affect the system performance, we should consider the measure as the mean cross-correlation value. Figures 14 and 15 summarize the peak auto-correlation values in terms of width of the main lobe i.e., range resolution and normalized mean cross-correlation values of different pulses, respectively.

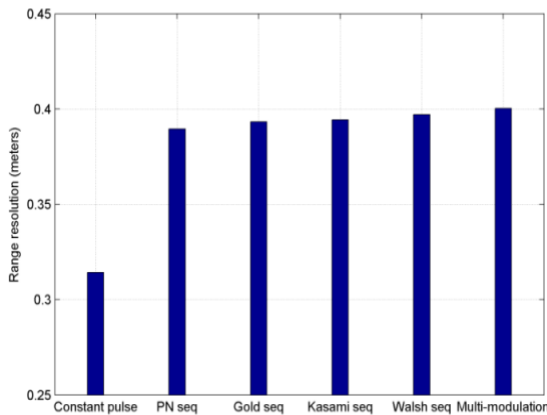


Fig. 14. Range resolution in terms of ACF.

### VII. SAR IMAGING IN JAMMING SCENARIOS

The scenario involves the SAR imaging in jamming scenarios by considering three distinct UWB-OFDM waveforms as SAR transmitted pulse. A DRFM repeat jammer will receive the radar transmitted pulse from the previous PRI, introduce a false delay and retransmit to radar at

next expected PRI to introduce false target in reconstructed SAR image. The objective is to investigate the performance of the UWB-OFDM waveform with constant pulse, noise-like pulses based on random sequences and multi-modulated waveform as SAR transmitted pulse in jamming scenarios.

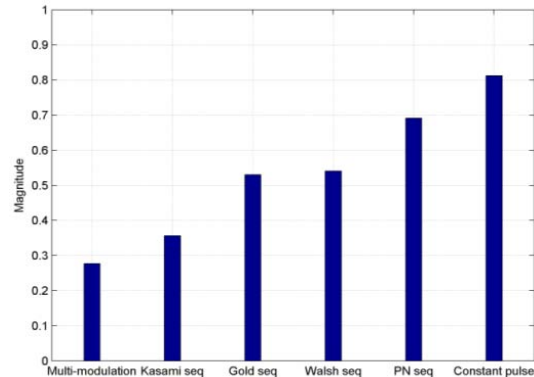


Fig. 15. Mean cross-correlation values.

Let us consider 2 point targets as actual target at the positions  $(x_n, y_n) = [(-300m, 80m), (300m, 80m)]$  and 2 point target as false target introduced by jammer at the positions  $(x_j, y_j) = [(-300m, -80m), (300m, -80m)]$ . Stripmap SAR topology is considered and UWB-OFDM waveform is used as transmitted pulse to perform the SAR raw data generation using while Range-Doppler algorithm (RDA) is used for SAR image reconstruction [15]. The details of SAR configuration can be found in [5]. Although different techniques exist in literature for SAR image reconstruction [16] RDA is chosen to achieve exact SAR transfer function.

Reconstructed SAR image with resolved point targets in jamming scenarios is shown in Fig. 16. Because of using UWB-OFDM waveform with constant pulse shape shown in Fig. 2 (a) as transmitted SAR signal at each PRI, the signal had strong correlation with the jammer transmitted signals causing both false targets presence at their respective positions in the reconstructed SAR image.

Point targets are also resolved by using UWB-OFDM waveform with random sub-carrier compositions shown in Fig. 3 as SAR transmitted pulse in jamming scenarios. Fig. 17 shows the reconstructed SAR image using a random waveform at each PRI. Because of transmitting a

unique UWB-OFDM signal at each PRI, the signal has weaker correlation with the jammer transmitted signals causing degraded false target appears in the reconstructed SAR image. Figure 18 shows the reconstructed SAR image using a unique UWB-OFDM waveform at each PRI employing multi-modulation technique as shown in Fig. 5. Because of transmitting a unique multi-modulated UWB-OFDM signal with high degree of randomness at each PRI, the signal has much weaker correlation with the jammer signals causing no false target appears in the reconstructed SAR image.

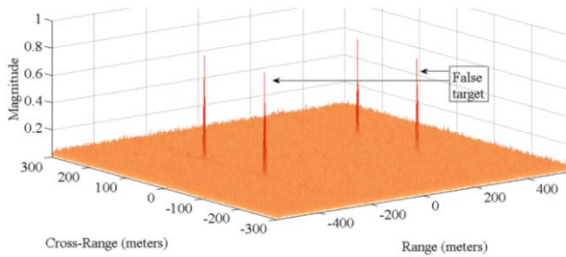


Fig. 16. SAR image showing two false targets.

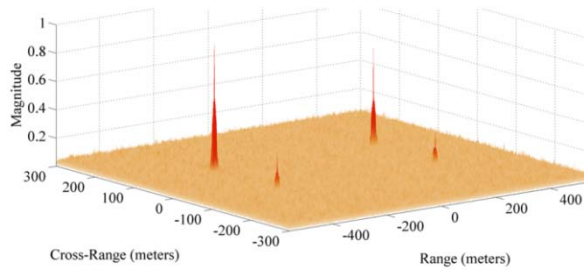


Fig. 17. SAR image showing degraded false targets.

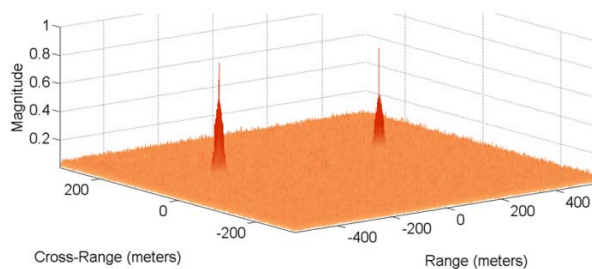


Fig. 18. SAR image without false targets.

The degradation of false targets using different sequences can be analyzed in terms of entropy [17] by analyzing SAR images i.e., degradation of

false targets will have reduction in entropy of the SAR image. Figure 19 shows the degradation of the false target in terms of entropy for different sequences as well as multi-modulation technique for different adaptivity factor. The adaptivity factor is the ratio of randomness of an UWB-OFDM waveform i.e., the ratio of 0's and 1's within the data vector that is used for waveform generation and is given by,

$$\eta = \frac{N_{0s}}{N_{sub}} \times 100 \quad (7)$$

where,  $N_{0s}$  is the number of zeros in the data vector and  $N_{sub}$  is the number of sub-carrier used in generating the waveform. As we are using BPSK modulation in case of random sequences, we should increase the number of 0's within the data vector to increase the adaptivity factor and vice versa.

In Fig. 19, we observe that as long as we increase the adaptivity factor, the entropy is increased. This is because the increment in the adaptivity factor increases the correlation of a pulse with the pulse at previous PRI. On the other hand, increment in the adaptivity factor increases the occupied bandwidth by the pulse, which in turns enhances the range resolution as shown in Fig. 20. We observe that multi-modulated UWB-OFDM waveform is the best choice for false target rejection but Kasami sequences exhibits a good balance between false target degradation as well as resolution among all random sequences.

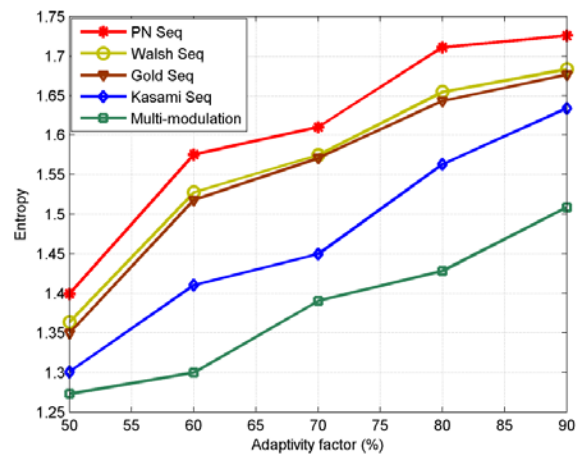


Fig. 19. Estimation of false target degradation.

UWB-OFDM waveform with constant pulse shape provides high-resolution SAR image but not effective for rejecting false target while UWB-

OFDM waveform with random sub-carrier orientation is capable of rejecting false target in jamming scenarios. On the other hand, UWB-OFDM waveform with multi-modulation technique is capable of rejecting false target completely. This waveform is evidently hardest to predict and intercept for the jammer because the signal is inherently multi-modulated. The high degree of randomness in SAR transmitted signal also rejects any reflected energy arrived from previous PRI during cross-correlation process as part of matched filtering, which in turns allow us to increase the swath. However, the trade-off is the increased target ambiguity i.e., increased main lobe width. This problem can be analyzed in terms of wide-band ambiguity function.

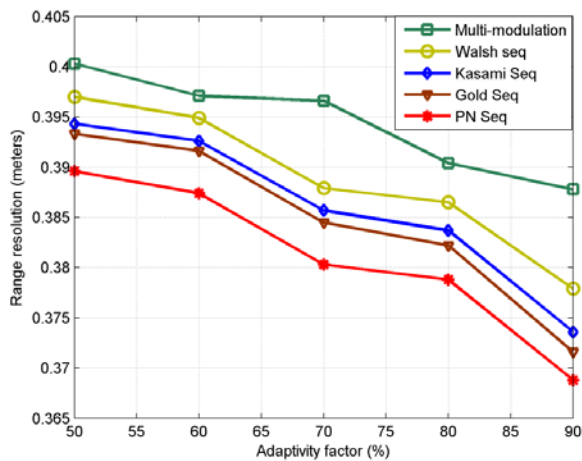


Fig. 20. Estimation of range resolution.

### VIII. WIDE-BAND AMBIGUITY FUNCTION (WAF)

Radar ambiguity function is used to evaluate the performance limitations of the chosen radar waveform. The ambiguity function (AF) for any waveform contains a main lobe whose maximum lies at AF (0, 0) with a spread in both Doppler and delay. The spread is determined by the signal duration ( $T_p$ ) and baseband bandwidth ( $B_0$ ). The delay spread is  $\tau = 1/B_0$  while the Doppler spread,  $\nu_0 = 1/T_p$ . In our case,  $T_p$  depends on the number of sub-carriers used in the OFDM signal. So, an OFDM signal with larger number of sub-carriers can produce a main lobe with a reduced Doppler ambiguity while increased sampling rate increases the baseband bandwidth, which in turns reduces main lobe delay ambiguity. The wideband

ambiguity function [18] suitable for UWB-OFDM radar signal is given by,

$$AF_{wb}(\alpha, t) = \sqrt{|\alpha|} \int_{-\frac{T_p}{2}}^{\frac{T_p}{2}} \Psi(t) \Psi^*(\alpha(t - \tau)) dt \quad (8)$$

where,  $\alpha = \frac{c-v}{c+v}$  and  $v$  is the radial velocity of the radar platform to the target and  $c$  is the speed of light. Equation (8) considers the Doppler shift of each sub-carrier individually whereas the narrowband AF considers only one sub-carrier causing incorrect Doppler shift for other sub-carriers. The continuous time analytical OFDM waveform [11] is given by,

$$\Psi(t) = \sum_{k=1}^N x(k) e^{j\left(\frac{2\pi kt}{T_p} + \phi_0(t)\right)} \quad 0 < t < T_p \quad (9)$$

where,  $x(k)$  is the  $k^{\text{th}}$  data symbol,  $N$  is the number of sub-carriers and  $T_p$  is the pulse duration. By substituting the analytical form of OFDM signal into equation (8), WAF for a UWB-OFDM signal is given by,

$$AF_{OFDM}(\alpha, \tau) = T_p \sqrt{|\alpha|} \sum_{l=1}^N \sum_{k=1}^N x(k) x(l) e^{j2\pi l \Delta f \alpha \tau} \text{sinc}(\pi \Delta f (k - l) T_p) \quad (10)$$

where, sub-carrier spacing  $\Delta f = 1/T_p$  has been substituted and  $\phi_0 = 0$  is assumed. Equation (10) shows the dependence of the AF on not only number of sub-carrier but also the orientation of the sub-carriers in the OFDM signal.

The range ambiguity can be reduced by increasing the adaptivity factor in UWB-OFDM SAR transmitted signal and is shown in Fig. 21. The reason behind this reduction in mainlobe width is that as long as we increase the adaptivity factor, the UWB-OFDM waveform approaches to the constant pulse shape as shown in Fig. 2. Figure 22 shows that the ambiguity in cross-range decreases as the number of sub-carrier increases. Increasing the number of sub-carrier in the signal has no effect on the main-lobe width because the bandwidth remains constant for any number of sub-carriers. However, increasing the number of sub-carriers will increase the size of raw SAR data, which should be minimized for radar processing purposes to reduce the computation time.

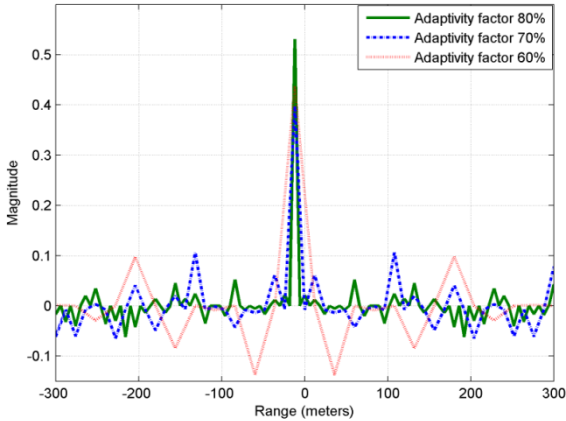


Fig. 21. Range ambiguity versus adaptivity factor.

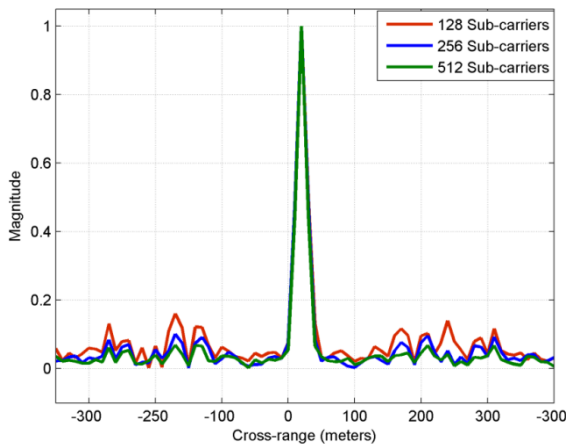


Fig. 22. Cross-range ambiguity versus number of OFDM sub-carriers.

Peak side-lobe (PSL) performance of a radar signal is a crucial part in determining whether a signal will be acceptable for high resolution imaging. PSL refers the maximum value residing outside the main-lobe. We are concerned with the difference between main-lobe peak and the highest side-lobe peak. Table 3 shows the normalized PSL performance for a varying number of sub-carriers and adaptivity factor. As expected, the PSL decreases as the number of sub-carriers and adaptivity factor increases.

## IX. CONCLUSION

Performance of UWB-OFDM based SAR imaging has been investigated in jamming scenarios. UWB-OFDM based SAR can be adapted with both friendly environments and with jamming scenarios just by changing the transmitted waveform. The adaptivity factor can

Table 3: OFDM sub-carrier versus PSL.

OFDM Sub-carriers	Peak side-lobe (dB)		
	Adaptivity factor 60%	Adaptivity factor 70%	Adaptivity factor 80%
128	-13.24	-16.14	-17.26
256	-16.02	-18.12	-21.04
512	-17.62	-19.03	-22.32

be used to handle mutual exclusion between resolution and false target rejection. The performance of the SAR system in both environments can easily be controlled by changing the number and composition of the OFDM sub-carriers. Wideband ambiguity function has been derived and the effect of adaptivity factor in UWB-OFDM waveform has been analyzed. The results prove that UWB technology enhances the resolution of SAR images while randomness of noise-like OFDM waveform improves the anti-jamming capabilities of SAR system. UWB-OFDM waveform with in addition with multi-modulation technique is an excellent choice to be used as SAR transmitted pulse in hostile environments to achieve secured SAR imaging.

## ACKNOWLEDGMENT

This work is funded by the National Plan for Science and Technology, Kingdom of Saudi Arabia, under project number: 08-ELE262-2.

## REFERENCES

- [1] M. Soumekh, *Synthetic Aperture Radar Signal Processing with MATLAB Algorithms*, 2<sup>nd</sup> ed. New York, USA: Wiley, 1999.
- [2] D. Garmatyuk and M. Brennehan, "Slow-time SAR signal processing for UWB OFDM radar system," *IEEE Radar Conf.*, Washington, USA, pp. 853-858, 2010.
- [3] R. Aiello and S. Wood, *Essentials of UWB*, 1<sup>st</sup> ed. New York: Cambridge, 2008.
- [4] K. P. Prokopidis and T. D. Tsiboukis, "Modeling of ground-penetrating radar for detecting buried objects in dispersive soils," *Appl. Comp. Electro. Society (ACES) Journal*, vol. 22, no. 2, pp. 287-294, 2007.
- [5] Md A. Hossain, I. Elshafiey, M. Alkanhal, and A. Mabrouk, "Adaptive UWB-OFDM synthetic aperture radar," *Proc. of Saudi Int. Electronics, Comm. and Photonics Conf. (SIEPCP)*, Riyadh, Saudi Arabia, pp. 1-6, 2011.

- [6] Md A. Hossain, I. Elshafiey, and M. Alkanhal, "High resolution UWB SAR based on OFDM architecture," *Proc. of 3<sup>rd</sup> Asia-Pacific Int. Conf. on Synthetic Aperture Radar (APSAR)*, Seoul, South Korea, pp. 1-4, 2011.
- [7] Md A. Hossain, I. Elshafiey, M. Alkanhal, and A. Mabrouk, "Anti-jamming capabilities of UWB-OFDM SAR," *Proc. of European Radar Conf. (EuRad)*, Manchester, United Kingdom, pp. 313-316, 2011.
- [8] Md A. Hossain, I. Elshafiey, M. Alkanhal, and A. Mabrouk, "Real-time implementation of UWB-OFDM synthetic aperture radar imaging," *IEEE Int. Conf. on Signal and Image Processing Applications (ICSIPA)*, Kuala Lumpur, Malaysia, pp. 450-455, 2011.
- [9] D. Garmatyuk, "Simulated imaging performance of UWB SAR based on OFDM," *Proc. of the IEEE Int. Conf. on Ultrawideband*, Waltham, MA, pp. 237-242, Sep. 24 - 27, 2006.
- [10] J. Schueger and D. S. Garmatyuk, "Multi-frequency OFDM SAR in presence of deception jamming," *EURASIP Journal on Adv. in Signal Processing*, pp. 1-13, 2010.
- [11] L. Hanzo and T. Keller, *OFDM and MC-CDMA*, 2<sup>nd</sup> ed. United Kingdom: Wiley, 2006.
- [12] M. Soumekh, "SAR-ECCM using phase-perturbated LFM chirp signals and DRFM repeat jammer penalization," *IEEE Trans. on Aerospace and Electronic Systems*, vol. 42, no. 1, pp. 191-205, Nov. 2006.
- [13] M. Richards, "Evaluating the radar cross section of maritime radar reflectors using computational electromagnetics," *Appl. Comp. Electro. Society (ACES) Journal*, vol. 24, no. 4, pp. 403-406, 2009.
- [14] D. U. Ke-lin and M. N. Swamy, *Wireless Communication Systems*, Cambridge University Press, New York, 2010.
- [15] I. G. Cumming and F. H. Wong, *Digital Processing of Synthetic Aperture Radar Data*, 2<sup>nd</sup> ed. United Kingdom: Artech House, 2004.
- [16] A. Capozzoli, C. Curcio, A. Lisenio, and P. Vinetti, "Fast interpolation accelerated on GPU for SAR back projection," *Proc. of the 28<sup>th</sup> Annual Rev. of Progress in Appl. Comp. Electro. Society (ACES)*, Columbus, OH, pp. 305-310, Apr. 2012.
- [17] R. C. Gonzalez and R. E. Woods, *Digital Image Processing*, 2<sup>nd</sup> Ed., Pearson Education, Inc. New Jersey, USA, 2008.
- [18] L. G. Weiss, "Wavelets and wideband correlation processing," *IEEE Signal Processing Magazine*, vol. 1, no. 11, pp. 13-32, Jan. 1994.



**Md Anowar Hossain** received his B.Sc. degree in Computer and Communication Engineering from International Islamic University Chittagong (IIUC), Bangladesh in 2005 and M.Sc. degree in Electrical Engineering from King Saud University, Saudi Arabia in 2012. He has been working as a researcher in the department of Electrical Engineering, King Saud University, from October 2008 to till now. Currently, he is pursuing PhD in Electrical Engineering at King Saud University. His research interests include UWB radar; synthetic aperture radar (SAR) imaging; radar jamming and anti-jamming; radar signal processing and FPGA based real-time signal processing.



**Ibrahim Elshafiey** received his B.Sc. degree in Communications and Electronics Engineering from Cairo University in 1985. He obtained his M.Sc. and PhD degrees from Iowa State University in 1992 and 1994, respectively. He is currently a professor in the Electrical Engineering Department, King Saud University, on loan from the Electrical Engineering Department, Fayoum University, Egypt. His research interests include computational electromagnetics, biomedical imaging and nondestructive evaluation.



**Majeed A. S. Alkanhal** received the B.Sc. and M.Sc. degrees from King Saud University, Riyadh, Saudi Arabia, in 1984 and 1986 respectively, and the PhD from Syracuse University, Syracuse, NY, in 1994, all in Electrical Engineering. He is presently a Professor and Chairman of the Electrical Engineering Department at King Saud University, Riyadh, Saudi Arabia. His research interests are in antennas and propagation, computational electromagnetics, and microwave engineering.